TOPOLOGICAL DERIVATIVE-BASED OPTIMIZATION OF MICRO-STRUCTURES CONSIDERING DIFFERENT MULTI-SCALE MODELS

E.A. DE SOUZA NETO, S. AMSTUTZ, S.M. GIUSTI, AND A.A. NOVOTNY

Abstract. A recently proposed algorithm for micro-structural optimization, based on the concept of topological derivative and a level-set domain representation, is applied to the synthesis of elastic and heat conducting bi-material micro-structures. The macroscopic properties are estimated by means of a family of multi-scale constitutive theories where the macroscopic strain and stress tensors (temperature gradient and heat flux vector in the heat conducting case) are defined as volume averages of their microscopic counterparts over a Representative Volume Element (RVE). Several finite element-based examples of micro-structural optimization are presented. Three multi-scale models, providing an upper and a lower bound for the macroscopic properties as well as the classical periodic medium solution, are considered in the optimization process. These models differ only in the kinematical constraints (thermal constraints in the heat conducting case) imposed on the RVE. The examples show that, in general, the obtained optimum micro-structure topology depends on the particular model adopted.

1. Introduction

The prediction of macroscopic heat conduction and mechanical properties of materials from the knowledge of their underlying microstructures has long been a subject of great interest in applied mechanics ([20, 21, 19, 8, 37, 13]). A particularly interesting branching of this field of research is the application of homogenization-based theories for the prediction of macroscopic properties in the design of microstuctures that produce in some sense an optimized macroscopic behaviour. The use of such theories in this context is reported, among others, by [38, 39, 25, 24]. In the methodology employed by these authors – which can now be regarded as conventional – the prediction of macroscopic properties is generally obtained through the concept of periodic homogenization, whose mathematical roots are traced back to the work of [8]. Of particular relevance here is the fact that the topology optimization algorithms in such cases rely invariably on some form of regularization of the problem posed by the topology change that occurs when a portion of the microscopic domain is replaced with either a void or a material whose properties differ from those of the original matrix. Despite their success in many reported applications, the main drawback of the regularization approach is probably the fact that it usually leads to relatively complex algorithms featuring on a number of problem-dependent artificial parameters and post-processing procedures for topology design.

In the present paper we adopt of a radically different approach that relies on *exact* formulae for the sensitivity of the macroscopic elastic and heat conducting responses to topological changes of the microscopic domain. These exact formulae have been proposed in [16] and [17] and rely on the concepts of *topological asymptotic analysis* and *topological derivative* ([40]) – which provide the correct mathematical framework for the calculation of sensitivities under singular topological changes typical of microstructural optimization problems. This concept has been successfully used, for example, in the topology optimization of load-bearing structures ([1, 3, 32]). Its main advantage lies in the fact that the sensitivities are obtained in exact form and, hence, allow the use of much simpler optimization algorithms which in particular do not rely on artificial algorithmic parameters. Here, the algorithm proposed by [3] is adapted for use in the microstructural optimization context. A series of numerical examples is presented which show the effectiveness of the approach. For comparison, three different homogenization-based models are used in the estimation of the macroscopic properties in the optimization problem. These models differ solely in the constraints imposed upon the possible displacement (or temperature) field of the microstructure and provide: the conventional periodic media prediction; an upper bound and; a lower bound for the elasticity (or conductivity) tensor.

Key words and phrases. Otimization of micro-structures, synthesis of micro-structures, multi-scale modelling, topological derivative, sensitivity analysis.

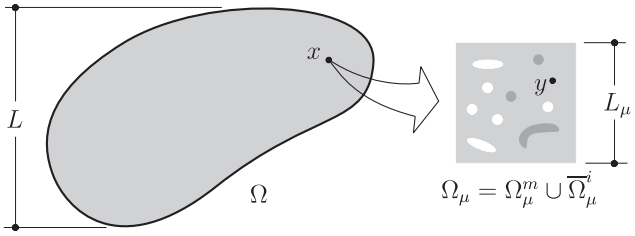

FIGURE 1. Macroscopic continuum with a locally attached microstructure.

The paper is organized as follows. The family of multi-scale constitutive theories used in the estimation of the elastic and heat conduction macroscopic constitutive responce is briefly described in Section 2. In Section 3 an overview of the topological derivative concept is given and the formulae for the topological derivatives of the macroscopic elasticity and heat conductivity tensors relevant to the present context are presented. The algorithm for topological optimization is briefly described in Section 3. The numerical examples are presented in Section 5 and, finally, some concluding remarks are made in Section 6.

2. Multi-scale constitutive modelling

This section reviews the multi-scale constitutive framework used here to estimate the macroscopic elasticity and thermal conductivity tensors from the knowledge of the underlying material microstructure. The approach is based on the ideas introduced by [13] and applied in the computational context, among others, by [28] and [29]. An axiomatic foundation for this class of models is discussed by [10]. The starting point of the theory is the assumption that any point x of the macroscopic continuum (refer to Fig.1) is associated to a local Representative Volume Element (RVE) whose domain Ω_μ, with boundary $\partial\Omega_\mu$, has characteristic length L_μ, much smaller than the characteristic length L of the macro-continuum domain, Ω. For the present purposes it is convenient to consider RVE domains consisting of a matrix Ω_μ^m, containing inclusions of different materials occupying a domain Ω_μ^i.

2.1. **The elasticity case.** Using the concept of *homogenization* the macroscopic strain tensor ε at a point x of the macroscopic continuum is defined as the volume average of its microscopic counterpart ε_μ over the domain of the RVE:

$$\varepsilon := \frac{1}{V_\mu}\int_{\Omega_\mu} \varepsilon_\mu = \frac{1}{V_\mu}\int_{\partial\Omega_\mu} u_\mu \otimes_s n, \tag{2.1}$$

where V_μ is the volume of the RVE, u_μ is the displacement field of the RVE, n is the outward unit normal to $\partial\Omega_\mu$, $\otimes_s$ denotes the symmetric tensor product and

$$\varepsilon_\mu = \nabla^s u_\mu. \tag{2.2}$$

Likewise, the macroscopic stress tensor σ, is defined as the volume average of the microscopic stress field σ_μ over the RVE, i.e.

$$\sigma := \frac{1}{V_\mu}\int_{\Omega_\mu} \sigma_\mu(u_\mu). \tag{2.3}$$

Without loss of generality, the field u_μ may be split into a sum

$$u_\mu(y) = u + \overline{u}_\mu(y) + \widetilde{u}_\mu(y)\ , \tag{2.4}$$

of a constant (rigid) RVE displacement coinciding with the macroscopic displacement $u(x)$, a field

$$\overline{u}_\mu(y) := \varepsilon y \tag{2.5}$$

and a displacement fluctuation field $\widetilde{u}_\mu(y)$ which, for convenience, is made to satisfy

$$\int_{\partial\Omega_\mu} \tilde{u}_\mu = 0. \tag{2.6}$$

With the split (2.4), the microscopic strain field can be written as a sum

$$\varepsilon_\mu = \varepsilon + \nabla^s \widetilde{u}_\mu\ , \tag{2.7}$$

of a homogeneous strain (uniform over the RVE) coinciding with the macroscopic strain and a field $\nabla^s \widetilde{u}_\mu$ corresponding to a fluctuation of the microscopic strain about the homogenized (average) value.

In the present paper we focus on RVEs consisting of a matrix Ω_μ^m, containing inclusions occupying a domain Ω_μ^i made of materials modelled as isotropic linear elastic. Hence, we have the constitutive law

$$\sigma_\mu(u_\mu) = \mathbb{C}_\mu \nabla^s u_\mu. \tag{2.8}$$

where $\mathbb{C}_\mu$ is the fourth-order isotropic elasticity tensor

$$\mathbb{C}_\mu = \frac{E_\mu}{1-\nu_\mu^2}\left[(1-\nu_\mu)\,\mathbb{I} + \nu_\mu\,(\mathrm{I}\otimes\mathrm{I})\right], \tag{2.9}$$

with I and $\mathbb{I}$ denoting the second- and fourth-order identity tensors, respectively, and E_μ and ν_μ the Young's modulus and Poisson ratio fields, here assumed to be given by

$$E_\mu := \left\{ \begin{array}{ccc} E_\mu^m & \text{if} & y \in \Omega_\mu^m \\ E_\mu^i & \text{if} & y \in \Omega_\mu^i \end{array} \right. \quad \text{and} \quad \nu_\mu := \left\{ \begin{array}{ccc} \nu_\mu^m & \text{if} & y \in \Omega_\mu^m \\ \nu_\mu^i & \text{if} & y \in \Omega_\mu^i. \end{array} \right. \tag{2.10}$$

The combination of (2.1), (2.4) and (2.8) together with the *Hill-Mandel Principle of Macro-Homogeneity* ([21, 27]) in the virtual work statement of equilibrium of the RVE, yields the *RVE mechanical Equilibrium Problem* which consists in finding, for a given macroscopic strain ε, an admissible displacement fluctuation field $\tilde{u}_\mu \in \mathcal{U}_\mu$ such that

$$\int_{\Omega_\mu} \sigma_\mu(\widetilde{u}_\mu) \cdot \nabla^s \eta = -\int_{\Omega_\mu} \sigma_\mu(\overline{u}_\mu) \cdot \nabla^s \eta \quad \forall \eta \in \mathcal{U}_\mu, \tag{2.11}$$

where the (as yet not defined) space $\mathcal{U}_\mu$ of kinematically admissible displacement fluctuation (and virtual displacement) fields of the RVE is a subspace of $\mathcal{U}_\mu^*$ – the minimally constrained space of kinematically admissible displacement fluctuations compatible with the strain averaging assumption (2.1):

$$\mathcal{U}_\mu \subset \mathcal{U}_\mu^* := \left\{ v \in [H^1(\Omega_\mu)]^2 : \int_{\Omega_\mu} v = 0\,, \int_{\partial\Omega_\mu} v \otimes_s n = 0 \right\}. \tag{2.12}$$

The macroscopic stress response is obtained by solving problem (2.11) for the given ε first and then using (2.4), (2.8) and (2.3) to calculate σ.

The characterization of a multi-scale model of the present type is completed with the choice of a suitable space $\mathcal{U}_\mu$ of kinematically admissible displacement fluctuations. The adopted space defines the kinematical constraints to be imposed upon the RVE and the resulting macroscopic constitutive response is generally dependent on this choice. Three commonly adopted choices are

- *Linear RVE boundary displacements* or simply *linear model*. For this class of models the choice is

$$\mathcal{U}_\mu = \mathcal{U}_\mu^{\mathcal{L}} := \left\{ \widetilde{u}_\mu \in \mathcal{U}_\mu^* : \widetilde{u}_\mu(y) = 0 \ \forall y \in \partial\Omega_\mu \right\}. \tag{2.13}$$

  The displacements on $\partial\Omega_\mu$ are $u_\mu = u + \varepsilon y$.
- *Periodic RVE boundary fluctuations model* or simply *periodic model*. This is typically associated with the modelling of periodic media. The RVE domain in this case has to satisfy geometrical constraints as the macroscopic continuum is generated by the periodic repetition of the RVE – here usually referred to as the unit cell. The space of kinematically admissible displacement fluctuations is defined as

$$\mathcal{U}_\mu = \mathcal{U}_\mu^{\mathcal{P}} := \left\{ \widetilde{u}_\mu \in \mathcal{U}_\mu^* : \widetilde{u}_\mu(y^+) = \widetilde{u}_\mu(y^-) \quad \forall (y^+, y^-) \in P \right\}, \tag{2.14}$$

  where P is the set of pairs of points on opposing sides of the boundary $\partial\Omega_\mu$ (fig. 2 illustrates a rectangular and a hexagonal RVE) defined to satisfy the periodicity constraint.

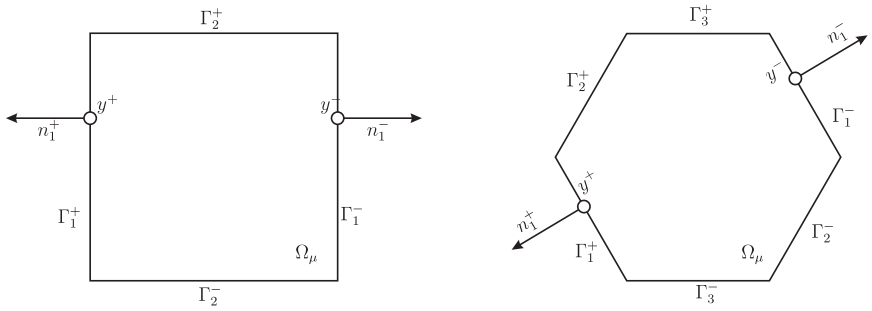

FIGURE 2. Typical RVE geometries for periodic media. Square and hexagonal cells.

- *Minimally constrained* or *uniform RVE boundary traction model*. In this case we impose the minimum kinematical constraint compatible with the strain averaging assumption:

$$\mathcal{U}_\mu = \mathcal{U}_\mu^{\mathcal{U}} := \mathcal{U}_\mu^*. \tag{2.15}$$

  It can be shown ([10]) that this choice of constraint produces a uniform traction field on $\partial\Omega_\mu$, i.e.

$$\sigma_\mu(y)\, n(y) = \sigma n(y) \quad \forall y \in \partial\Omega_\mu, \tag{2.16}$$

  where σ is the macroscopic stress tensor.

Remark 1. *Note that the spaces of displacement fluctuations (and virtual displacement) listed above satisfy*

$$\mathcal{U}_\mu^{\mathcal{L}} \subset \mathcal{U}_\mu^{\mathcal{P}} \subset \mathcal{U}_\mu^{\mathcal{U}}. \tag{2.17}$$

Then, in general, in the solution of the equilibrium problem (2.11) the choice of the linear boundary displacement constraint produces the stiffest solution whereas the minimaly constrained kinematics assumption produces the most compliant one. In this sense, within this multi-scale framework the use of the linear and the minimum constraint provide, respectively, an upper and a lower bound for the response of the material. The use of these bounds as well as the (generally intermediate) prediction obtained under the periodicity assumption in the synthesis of microstructures will be discussed in section 5.

A closed formula for the macroscopic elasticity tensor $\mathbb{C}$ can be easily obtained by conveniently re-writing (2.11) as a superposition of linear problems associated with the individual Cartesian components of the macroscopic strain tensor ([28]). The final formula reads

$$\mathbb{C} = \overline{\mathbb{C}} + \widetilde{\mathbb{C}}, \tag{2.18}$$

where $\overline{\mathbb{C}}$ is the volume average elasticity tensor:

$$\overline{\mathbb{C}} = \frac{1}{V_\mu} \int_{\Omega_\mu} \mathbb{C}_\mu, \tag{2.19}$$

and $\widetilde{\mathbb{C}}$ is a contribution that depends generally on the choice of space $\mathcal{U}_\mu$:

$$\widetilde{\mathbb{C}} := \left[\frac{1}{V_\mu} \int_{\Omega_\mu} (\sigma_\mu(\widetilde{u}_{\mu_{kl}}))_{ij} \right] (e_i \otimes e_j \otimes e_k \otimes e_l) \ , \tag{2.20}$$

where $\{e_i\}$ is the orthonormal basis of the Euclidean space and $(\sigma_\mu(\widetilde{u}_{\mu_{kl}}))_{ij}$ denotes the ij-component of the fluctuation stress associated with the displacement fluctuation field $\widetilde{u}_{\mu_{kl}} \in \mathcal{U}_\mu$ that solves the linear variational equation

$$\int_{\Omega_\mu} \sigma_\mu(\widetilde{u}_{\mu_{kl}}) \cdot \nabla^s \eta = -\int_{\Omega_\mu} \mathbb{C}_\mu(e_k \otimes e_l) \cdot \nabla^s \eta \quad \forall \eta \in \mathcal{U}_\mu \ , \tag{2.21}$$

for $k, l = 1, 2$ (in the two-dimensional case).

2.2. **The heat conduction case.** Multi-scale constitutive theories to predict the heat conductivity properties of materials whose constituents are modelled by the Fourier Law can be obtained within a framework completely analogous to that of linear elastic materials described in the above. In the heat conduction case, the fundamental macroscopic quantities taken as volume averages of the microscopic counterpart fieds can be chosen as the temperature gradient and the heat flux:

$$\nabla_x \theta := \frac{1}{V_\mu} \int_{\Omega_\mu} \nabla \theta_\mu \tag{2.22}$$

and

$$q := \frac{1}{V_\mu} \int_{\Omega_\mu} q_\mu \tag{2.23}$$

where θ and q denote, respectively, macroscopic temperature and heat flux and θ_μ and q_μ are the corresponding microscopic fields of the RVE. This approach follows closely that of [13] and has been recently employed by [34] and [18].

Similarly to (2.4), without loss of generality, the microscopic temperature field θ_μ can be split into a sum

$$\theta_\mu(y) = \theta + \overline{\theta}_\mu(y) + \widetilde{\theta}_\mu(y), \tag{2.24}$$

of a constant temperature field (coinciding with the macrosopic temperature $\theta(x)$), a homogeneous gradient temperature field, $\overline{\theta}_\mu(y) := \nabla_x \theta \cdot y$, and a temperature fluctuation field, $\widetilde{\theta}_\mu(y)$. In addition, we also assume that

$$\theta = \frac{1}{V_\mu} \int_{\Omega_\mu} \theta_\mu. \tag{2.25}$$

Following the split (2.24), the microscopic temperature gradient can be expressed as a sum

$$\nabla \theta_\mu = \nabla_x \theta + \nabla \widetilde{\theta}_\mu, \tag{2.26}$$

of a homogeneous gradient (uniform over the RVE) coinciding with the macroscopic temperature gradient and a field $\nabla \widetilde{\theta}_\mu$ corresponding to a fluctuation of the microscopic temperature gradient about the homogenised value.

Crucial to the theory is a heat conduction version of the classical Hill-Mandel Principle of Macro-Homogeneity for solids ([21, 27]). Here we postulate the following analogous relation ([18]):

$$q \cdot \nabla_x \theta = \frac{1}{V_\mu} \int_{\Omega_\mu} q_\mu \cdot \nabla \theta_\mu, \tag{2.27}$$

which must hold for any admissible microscopic temperature field.

Remark 2. *Equation (2.27) is at variance with Germain* et al. [13] *who postulated the following micro-macro dissipation equivalence relation:*

$$q \cdot \frac{\nabla_x \theta}{\theta} = \frac{1}{V_\mu} \int_{\Omega_\mu} q_\mu \cdot \frac{\nabla \theta_\mu}{\theta_\mu}, \tag{2.28}$$

as the heat conduction counterpart of the original mechanical Hill-Mandel Macro-homogeneity Principle. We remark, however, that the use of (2.27) can be justified as follows. Firstly, recall that the basic requirement of positive thermal dissipation at the macro-scale, imposed by the second law of thermodynamics, is expressed by

$$-q \cdot \frac{\nabla_x \theta}{\theta} \geq 0. \tag{2.29}$$

Analogously, at the micro-scale, the inequality

$$-q_\mu \cdot \frac{\nabla \theta_\mu}{\theta_\mu} \geq 0, \tag{2.30}$$

must hold point-wise. If (2.30) indeed holds point-wise at the RVE level, then, trivially, since θ_μ is positive,

$$-q_\mu \cdot \nabla \theta_\mu \geq 0. \tag{2.31}$$

The use of (2.27) ensures, in turn, that

$$-q \cdot \nabla_x \theta \geq 0, \tag{2.32}$$

so that the macroscopic dissipation inequality (2.29) holds at the corresponding macro-continuum point. In summary, if positive dissipation is assured point-wise at the RVE level, then version (2.27) of the Hill-Mandel Principle of Macro-homogeneity for heat conduction problems ensures positive dissipation at the macroscopic level.

In the present work, we focus on microstructures whose constituents' heat conduction behaviour is modelled by the classical Fourier Law:

$$q_\mu(\theta_\mu) = -\mathbf{K}_\mu \nabla\theta_\mu, \tag{2.33}$$

where $\mathbf{K}_\mu$ is the microscopic heat conductivity tensor field. In particular, we shall model the matrix and inclusions as two distinct homogeneous isotropic materials, so that

$$\mathbf{K}_\mu = k_\mu \,\mathrm{I} := \begin{cases} k_\mu^m \,\mathrm{I} & \text{if} \quad y \in \Omega_\mu^m \\ \\ k_\mu^i \,\mathrm{I} & \text{if} \quad y \in \Omega_\mu^i, \end{cases} \tag{2.34}$$

where k_μ^m and k_μ^i denote, respectively, the thermal conductivity coefficients of the matrix and inclusions materials.

The additive decomposition of θ_μ together with Fourier Law gives

$$q_\mu(\theta_\mu) = q_\mu(\overline{\theta}_\mu) + q_\mu(\widetilde{\theta}_\mu)\,, \tag{2.35}$$

where $q_\mu(\overline{\theta}_\mu)$ is a uniform thermal flux field and $q_\mu(\widetilde{\theta}_\mu)$ is a thermal flux fluctuation field associated with the temperature fluctuation $\widetilde{\theta}_\mu$.

In a manner completely analogous to that of linear elastic microstuctures, by combining the classical variational statement of thermal equilibrium with postulate (2.27) and the additive split (2.26), we obtain ([18]) the *RVE thermal equilibrium problem* which consists of finding, for a given macroscopic temperature gradient $\nabla\theta$, an admissible temperature fluctuation field $\widetilde{\theta}_\mu \in \mathcal{V}_\mu$ such that

$$\int_{\Omega_\mu} q_\mu(\widetilde{\theta}_\mu) \cdot \nabla\eta = -\int_{\Omega_\mu} q_\mu(\overline{\theta}_\mu) \cdot \nabla\eta \quad \forall \eta \in \mathcal{V}_\mu, \tag{2.36}$$

where $\mathcal{V}_\mu$ denotes the (yet to be chosen) functional space of admissible temperature fluctuation fields (and virtual temperatures) that define the thermal constraint assumed within the RVE. The space $\mathcal{V}_\mu$ must be a subspace of the minimally constrained space $\mathcal{V}_\mu^*$ of temperature fluctuations compatible with the temperature gradient averaging assumption (2.22):

$$\mathcal{V}_\mu \subset \mathcal{V}_\mu^* := \left\{ v \in H^1(\Omega_\mu) : \int_{\Omega_\mu} v = 0,\ \int_{\partial\Omega_\mu} v\, n = 0 \right\}. \tag{2.37}$$

Possible definitions of $\mathcal{V}_\mu$ analogous to (2.13–2.15) used in the mechanical multi-scale model are

- *Linear RVE boundary temperature model* or simply *linear model*. The choice here is

$$\mathcal{V}_\mu = \mathcal{V}_\mu^{\mathcal{L}} := \left\{ \widetilde{\theta}_\mu \in \widetilde{\mathcal{W}}_\mu^* : \widetilde{\theta}_\mu(y) = 0 \quad \forall y \in \partial\Omega_\mu \right\}. \tag{2.38}$$

- *Periodic RVE boundary fluctuations model* or simply *periodic model*. In this case,

$$\mathcal{V}_\mu = \mathcal{V}_\mu^{\mathcal{P}} := \left\{ \widetilde{\theta}_\mu \in \widetilde{\mathcal{W}}_\mu^* : \widetilde{\theta}_\mu(y^+) = \widetilde{\theta}_\mu(y^-) \quad \forall (y^+, y^-) \in P \right\}. \tag{2.39}$$

- *Minimally constrained* or *Uniform normal RVE boundary heat flux model*. In this case, the choice is

$$\mathcal{V}_\mu = \mathcal{V}_\mu^{\mathcal{U}} := \mathcal{V}_\mu^*. \tag{2.40}$$

  It can be shown ([18]) that this definition implies a uniform normal flux on the boundary of the RVE:

$$q_\mu(y) \cdot n(y) = q \cdot n(y) \quad \forall y \in \partial\Omega_\mu. \tag{2.41}$$

  where q is the macroscopic heat flux vector.

Remark 3. *Similarly to the comments made in Remark 1, we have*

$$\mathcal{V}_\mu^{\mathcal{L}} \subset \mathcal{V}_\mu^{\mathcal{P}} \subset \mathcal{V}_\mu^{\mathcal{U}}. \tag{2.42}$$

It has been shown by [33] *that the linear boundary temperature and uniform boundary flux models lead, respectively, to an upper and a lower bound for the macroscopic conductivity tensor.*

Finally, a closed form for the macroscopic heat conductivity tensor can be obtained in a completely analogous manner to that of the elasticity case. The final formula is

$$\mathbf{K} = \overline{\mathbf{K}} + \widetilde{\mathbf{K}}, \tag{2.43}$$

where

$$\overline{\mathbf{K}} = \frac{1}{V_\mu} \int_{\Omega_\mu} \mathbf{K}_\mu \tag{2.44}$$

is the volume average conductivity tensor and $\widetilde{\mathbf{K}}$ is the contribution associated to the choice of space $\mathcal{V}_\mu$, given by

$$\widetilde{\mathbf{K}} := \left[\frac{1}{V_\mu} \int_{\Omega_\mu} (q_\mu(\widetilde{\theta}_{\mu_j}))_i \right] e_i \otimes e_j \,, \tag{2.45}$$

where $(q_\mu(\widetilde{\theta}_{\mu_j}))_i$ is the i-component of the microscopic flux fluctuation field associated with the temperature fluctuation $\widetilde{\theta}_{\mu_j} \in \mathcal{V}_\mu$ that solves

$$\int_{\Omega_\mu} q_\mu(\widetilde{\theta}_{\mu_j}) \cdot \nabla \eta = -\int_{\Omega_\mu} \mathbf{K}_\mu e_j \cdot \nabla \eta \quad \forall \eta \in \mathcal{V}_\mu. \tag{2.46}$$

for $j = 1, 2$.

3. Topology sensitivity of the homogenized elasticity and conductivity tensors

Crucial to the algorithm used here in the topology optimization of microstructures are the mathematical concepts of topological asymptotic analysis and topological derivative. These concepts have been originally introduced by [40] and provide the correct mathematical framework whereby *exact* expressions may be derived for the sensitivity of functionals whose value depend on a given domain to singular topological changes of the domain. The notion of topological derivative has proved extremely useful in the treatment of a wide range of problems in mechanics, optimization, inverse analysis and image processing (see for instance, [4, 9, 12, 22, 23, 31, 32]). Here, we apply this concept to problems of microstructural optimization where the underlying cost functions are defined in terms of the homogenized elasticity and heat conductivity tensors discussed in the previous section.

The topological derivative is an extension of the conventional notion of derivative. The main idea is briefly reviewed in the following. Let ψ be a generic functional whose value depends on a given domain and let it have sufficient regularity so that the following expansion is possible

$$\psi(\rho) = \psi(0) + f(\rho)\, D_T\psi + o(f(\rho)), \tag{3.1}$$

where $\psi(0)$ is the value of the functional for a domain Ω and $\psi(\rho)$ is the value of the functional for a domain Ω^ρ that differs from Ω by a topological perturbation of size ρ. The non-negative scalar ρ parametrizes the domain so that the original domain Ω is retrieved when $\rho = 0$. In addition, $f(\rho)$ is a *function* such that $f(\rho) \to 0$ with $\rho \to 0^+$ and $o(f(\rho))$ contains all terms of higher order in $f(\rho)$. Expression (3.1) is the *topological asymptotic expansion* of ψ and $D_T\psi$ is defined as the *topological derivative* of ψ at the unperturbed (or original) domain Ω. For the study of asymptotic expansion of inclusion of finite size, we refer the reader to [35, 11] and [45].

In the present context, the domain of interest is the RVE doman and the primary functionals whose topological derivatives are needed are the two-dimensional macroscopic elasticity and heat conductivity tensors, $\mathbb{C}$ and $\mathbf{K}$. The dependence of these functionals on the domain of the RVE is defined through relations (2.18–2.21) and (2.43–2.46), respectively. The topological perturbation to be considered consists of the introduction of a circular inclusion of radius ρ centred at an arbitrary point $\hat{y} \in \Omega_\mu$. More precisely, the perturbed domain is obtained by first introducing a circular hole $\mathcal{H}_\rho$ of radius ρ centred at $\hat{y} \in \Omega_\mu$ and, then, replacing this region with a circular inclusion $\mathcal{I}_\rho$ of a different material property. The topologically perturbed domain is defined as (see to Fig. 3)

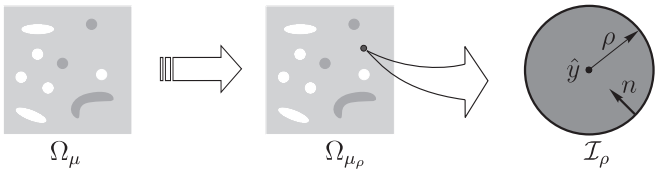

FIGURE 3. Topological perturbation at the microscopic level.

$$\Omega_\mu^\rho = \left(\Omega_\mu \backslash \overline{\mathcal{H}_\rho}\right) \cup \mathcal{I}_\rho, \tag{3.2}$$

with the corresponding microscopic constitutive tensor fields given by

$$\mathbb{C}_\mu^\rho = \begin{cases} \mathbb{C}_\mu & \text{in} \quad \Omega_\mu \setminus \overline{\mathcal{H}_\rho} \\ \gamma_{\mathbb{C}}\mathbb{C}_\mu & \text{in} \quad \mathcal{I}_\rho, \end{cases} \quad \text{and} \quad \mathbf{K}_\mu^\rho = \begin{cases} \mathbf{K}_\mu & \text{in} \quad \Omega_\mu \setminus \overline{\mathcal{H}_\rho} \\ \gamma_{\mathbf{K}}\mathbf{K}_\mu & \text{in} \quad \mathcal{I}_\rho, \end{cases} \tag{3.3}$$

where the (given) scalar parameters $\gamma_{\mathbb{C}}, \gamma_{\mathbf{K}} \in \Re^+$ define the contrast between the constitutive responses of matrix and inclusion.

The topological derivatives of $\mathbb{C}$ and $\mathbf{K}$ with respect to perturbations of the above type are given in the following theorems.

Theorem 4. *The topological asymptotic expansion of the macroscopic elasticity tensor in the present context is given by*

$$\mathbb{C}^\rho = \mathbb{C} + \frac{\pi\rho^2}{V_\mu} D_T\mathbb{C} + o(\rho^2), \tag{3.4}$$

where $\mathbb{C}^\rho$ denotes the macroscopic elasticity tensor associated with the topologically perturbed RVE domain Ω_μ^ρ and the fourth order tensor field $D_T\mathbb{C}$ over Ω_μ is the topological derivative of $\mathbb{C}$ at the unpertubed domain Ω_μ. Its explicit formula is

$$D_T\mathbb{C} = \mathbb{H}\sigma_\mu(u_{\mu_{ij}}) \cdot \sigma_\mu(u_{\mu_{kl}}) \; (e_i \otimes e_j \otimes e_k \otimes e_l), \tag{3.5}$$

with the canonical stress tensors $\sigma_\mu(u_{\mu_{ij}})$ given by

$$\sigma_\mu(u_{\mu_{ij}}) = \mathbb{C}_\mu(e_i \otimes e_j) + \sigma_\mu(\widetilde{u}_{\mu_{ij}}) \tag{3.6}$$

where $\widetilde{u}_{\mu_{ij}}$ are the solutions to the set of canonical variational problems (2.21). The isotropic fourth-order tensor $\mathbb{H}$ is defined as

$$\mathbb{H} = -\frac{1}{E_\mu}\left(\frac{1-\gamma_{\mathbb{C}}}{1+\alpha\gamma_{\mathbb{C}}}\right)\left[4\mathbb{I} - \frac{1-\gamma_{\mathbb{C}}(\alpha-2\beta)}{1+\beta\gamma_{\mathbb{C}}}\,(\mathrm{I}\otimes\mathrm{I})\right], \tag{3.7}$$

with

$$\alpha = \frac{1+\nu_\mu}{1-\nu_\mu} \quad \textit{and} \quad \beta = \frac{3-\nu_\mu}{1+\nu_\mu}\,. \tag{3.8}$$

Proof. A complete proof of this theorem is given in [15]. □

Theorem 5. *The topological asymptotic expansion of the macroscopic thermal conductivity tensor in the present context reads*

$$\mathbf{K}^\rho = \mathbf{K} + \frac{\pi\rho^2}{V_\mu} D_T\mathbf{K} + o(\rho^2)\,, \tag{3.9}$$

where $\mathbf{K}^\rho$ is the macroscopic heat conductivity tensor for the perturbed domain Ω_μ^ρ and the second-order tensor field $D_T\mathbf{K}$ is the topological derivative of $\mathbf{K}$ at the unperturbed domain Ω_μ:

$$D_T\mathbf{K} = -2k_\mu \frac{1-\gamma_{\mathbf{K}}}{1+\gamma_{\mathbf{K}}} \nabla\theta_{\mu_i} \cdot \nabla\theta_{\mu_j} \; (e_i \otimes e_j)\,, \tag{3.10}$$

with $\nabla\theta_{\mu_i}$ the canonical microscopic temperature gradient fields given by

$$\nabla\theta_{\mu_i} = \nabla_x\theta \cdot e_i + \widetilde{\theta}_{\mu_i}, \tag{3.11}$$

where the scalars $\widetilde{\theta}_{\mu_i}$ are the solutions of the canonical variational problems (2.46).

Proof. A proof of this theorem is given in [18]. □

Remark 6. *The value of the topological derivative of the macroscopic elasticity (heat conductivity) tensor at an arbitrary point $\hat{y} \in \Omega_\mu$ is a rigorous first-order approximation in the volume fraction of inclusion to the change in the macroscopic elasticity (heat conductivity) tensor resulting from the insertion of an inclusion of given contrast $\gamma_{\mathbb{C}}$ ($\gamma_{\mathbf{K}}$) centred at $\hat{y}$.*

4. Topological derivative-based microstucture optimization algorithm

The information provided by the topological derivative (see Remark 6) is of an obvious appeal in the derivation of topology optimization procedures. Such a concept has been recently used with success, for example, in the topology optimization of load-bearing structures ([1, 3, 32, 43]). Since a rigorous first-order accurate measure of the variation of the cost function due to domain topology changes is available in closed form, algorithms based on this concept are remarkably simpler than procedures based on the regularization of the problem posed by the singular change of a material point (or region) into a different material or a hole ([39, 25, 7, 6]). In particular, they do not require the use of artificial algorithmic parameters or post-processing strategies common to regularized approaches.

In the present paper, we apply these ideas to the topology optimization/synthesis of bi-material elastic and heat conducting microstructures consisting of the materials we refer to as matrix and inclusion. The basic problems considered are of the following types:

$$\underset{\Omega_\mu^m \subset \Omega_\mu}{\text{Minimize}}\; J(\Omega_\mu^m) = h(\mathbf{K}) + \lambda \frac{V_\mu^m}{V_\mu} \;, \tag{4.1}$$

in the optimization of the macroscopic elastic properties, and

$$\underset{\Omega_\mu^m \subset \Omega_\mu}{\text{Minimize}}\; J(\Omega_\mu^m) = h(\mathbb{C}) + \lambda \frac{V_\mu^m}{V_\mu} \;, \tag{4.2}$$

in the optimization of the macroscopic heat conduction properties. Here, J is a cost functional whose argument is the domain Ω_μ^m occupied by the matrix material, h is a scalar-valued function of either the macroscopic elasticity tensor or the macrosopic heat conductivity tensor which, in turn, are functionals of the domain Ω_μ^m defined respectively through relations (2.18–2.21) and (2.43–2.46). The fixed parameter λ is a Lagrange multiplier used to impose a constraint on the volume fraction V_μ^m/V_μ of matrix material in the RVE.

In the above defined problems, function h effectively defines what overall property is to be optimized. With $D_T\mathbb{C}$ (or $D_T\mathbf{K}$) at hand, the exact topological derivative field of h – the derivative of of h with respect to the volume fraction of a newly inserted inclusion of given contrast – can be obtained by a straightforward application of the conventional rules of differential calculus. Accordingly, the topological derivative of the cost functional J is given by

$$D_T J = \langle Dh, D_T(\mathbf{K}) \rangle + \lambda \;. \tag{4.3}$$

in the problem of optimization of elastic properties, and

$$D_T J = \langle Dh, D_T(\mathbb{C}) \rangle + \lambda \;. \tag{4.4}$$

in the optimization of heat conductivity properties, where Dh denotes the (conventional) derivative of h with respect to its argument and $\langle \cdot, \cdot \rangle$ the appropriate product.

4.1. The algorithm.

The algorithm used in Section 5 in the solution of problems of type (4.1) and (4.2) has been originally proposed and applied by [3] to topology optimization in the context of two-dimensional elasticity and flow through porous media. The procedure relies crucially on the use of the topological derivative of the cost function to define a feasible descent direction together with a level-set domain representation. Of particular relevance is the fact that the algorithm is of very simple computational implementation and, in addition, shows a remarkable ability to produce general topological domain changes rather uncommon in this context.

With the adoption of a level-set domain representation, the current domain Ω_μ^m is defined by a level-set function $\psi \in L^2(\Omega_\mu)$ such that

$$\Omega_\mu^m = \{ y \in \Omega_\mu \,|\, \psi(y) < 0 \}, \tag{4.5}$$

whereas the domain occupied by the inclusion material is defined as

$$\Omega_\mu^i = \{ y \in \Omega_\mu \,|\, \psi(y) > 0 \}. \tag{4.6}$$

A sufficient condition for local optimality in the present case ([3]) is that the following equivalence relation holds:

$$\exists\, \tau > 0 \quad \text{such that} \quad g = \tau\, \psi, \tag{4.7}$$

where the field g over the RVE domain is defined as

$$g := \begin{cases} -D_T J(\Omega_\mu^m)(y) & \text{if } \ y \in \Omega_\mu^m \\ \quad D_T J(\Omega_\mu^m)(y) & \text{if } \ y \in \Omega_\mu^i. \end{cases} \tag{4.8}$$

Starting from a given initial guess ψ_0 for the level-set function (correponding to an initial guess to the topology of the RVE) the algorithm generates a sequence of level-set functions (a sequence of RVE topologies) whose aim is to satisfy (4.7) or, equivalently,

$$\theta := \arccos\left[\frac{\langle g, \psi\rangle}{\|g\|_{L^2}\, \|\psi\|_{L^2}}\right] = 0, \tag{4.9}$$

approximately, where θ is the angle between the vectors g and ψ in $L^2(\Omega_\mu)$. Without loss of generality, ψ_0 is chosen as a unit vector of $L^2(\Omega_\mu)$. The algorithmic iterations are defined by the update formula

$$\psi_{n+1} = \frac{1}{\sin\theta_n}\left\{\sin[(1-k_n)\theta_n]\psi_n + \sin(k_n\theta_n)\frac{g_n}{\|g_n\|_{L^2}}\right\}, \quad n = 0, 1, 2, \cdots, \tag{4.10}$$

where $k_n \in [0, 1]$ is a step size determined by a simple line-search procedure in order to decrease the value of the cost function. By construction, (4.10) produces a sequence of level-set functions of unit L^2 norm.

A standard finite element approximation is used in the calculation of $\mathbb{C}$ (or $\mathbf{K}$). Details of implementation of the RVE constraints are given in [14]. The topological derivatives (3.5) or (3.10) are computed first within each element and then extrapolated/smoothed in a standard fashion to the nodes of the mesh. The same global finite element shape functions are used to define the level-set functions. The material properties are also assigned to nodes. Hence, nodes for which $\psi < 0$ are assigned the properties of the matrix material and nodes with $\psi > 0$ the properties of the inclusion material. The iterations (4.10) are assumed to have converged when, for some n, the angle θ_n is smaller than a pre-specified tolerance.

5. Examples. Topological optimization of micro-structures

Numerical examples of optimization of macroscopic elastic and heat conduction properties are presented in this section. The algorithm outlined in the preceeding section is used. For comparison, in all examples the optimization procedure is carried out having the linear, periodic and minimally constrained models as the underlying theories whereby the macroscopic properties to be optimized are estimated. As we shall see, different multi-scale models lead in general to different optimized microstructures.

In all cases the RVE geometry is a unity square $\Omega_\mu = (0, 1) \times (0, 1)$. The initial guess for the level-set function corresponds to a uniform matrix containing a circular disc of inclusion material with radius $r = 0.25$ centred at the centre of the RVE (see fig. 4(a)). The dark- and light-coloured areas correspond respectively to the matrix and inclusion domains. For the heat conduction cases the heat conductivities of the phases of the microstructure are $k_\mu^m = 1$ and $k_\mu^i = 0.01$. For the elasticity cases, the Young's moduli and Poisson ratios are given by $E_\mu^m = 1$, $E_\mu^i = 0.01$ and $\nu_\mu^m = \nu_\mu^i = 0.3$. That is, in both types of problems a contrast parameter of 0.01 is used. In all examples, a coarser uniform mesh (fig. 4(b)) with 3281 nodes and 6400 three-noded triangular elements is used first. When convergence is achieved, a uniform mesh refinement step is perfomed and the algorithm executed again to convergence taking the topology of the coarser mesh as the initial guess. This process is repeated until convergence is achieved with a final mesh of high resolution containing 205441 nodes and 409600 elements. The convergence criterion adopted is $\theta \leq 1^\circ$.

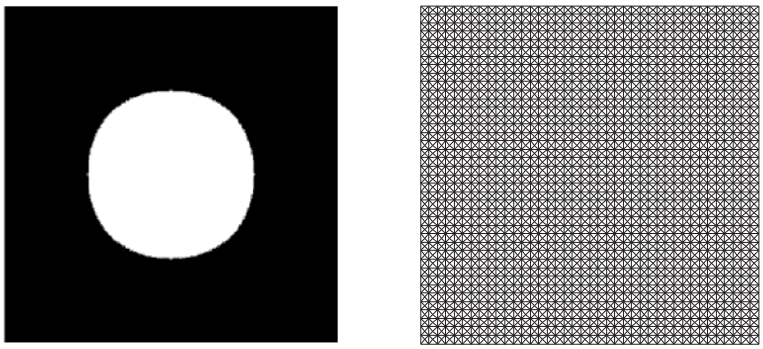

(a) (b)

FIGURE 4. (a) Initial guess for optimum topology, and; (b) Inital mesh.

5.1. **Horizontal heat conductivity maximization.** In this first example, we wish to maximize the macroscopic heat conductivity in the horizontal direction. Accordingly we define simply

$$h(\mathbf{K}) := (\mathbf{K}^{-1})_{11}. \tag{5.1}$$

The Lagrange multiplier is taken as $\lambda = 45$. The resulting optimized topologies are shown in fig. 5 and the evolution of the cost function during the iterations is shown in fig. 6.

(a) linear model (b) periodic model (c) uniform model

FIGURE 5. Maximization of the horizontal heat conductivity. Optimized RVE topologies

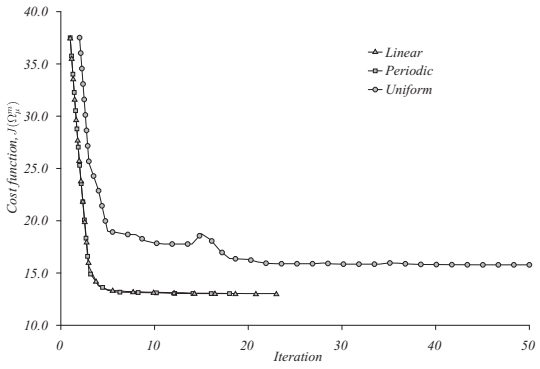

FIGURE 6. Horizontal heat conductivity maximization. Convergence history.

The topologies presented in figs. 5(a) 5(b) coincide with the classical topologies proposed by [44] and [36] in the context of linear elastic microstructures. To derive the well-established lower and upper

bounds for overall elastic constants, these authors considered the microcell composed of strips of two different materials. In the present context of heat conductivity, the upper (lower) bound is obtained when the strips are aligned with (orthogonal to) the direction of the heat flux. The present result obviously corresponds to the upper bound. It is worth noting that the microstructure generated under the minimal RVE constraint assumption, shown in fig. 6(c), is of much greater complexity than the ones obtained under the the more constraining periodicity and linear boundary temperature assumptions.

5.2. **Orthotropic heat conductivity maximization.** The aim here is to maximize the heat conductivity in the horizontal and vertical directions simultaneously. Here the volume fraction of the inclusion phase is fixed as 0.422 and the parameter λ is obtained accordingly. The function $h(\mathbf{K})$ is defined as

$$h(\mathbf{K}) := \tfrac{1}{2}[(\mathbf{K}^{-1})_{11} + (\mathbf{K}^{-1})_{22}]. \tag{5.2}$$

The optimized topologies obtained in this case are shown in fig. 7 and the convergence history in fig. 8. The topologies obtained for the periodic and uniform boundary flux models, shown respectively in figs. 7(b) and 7(c), are similar to that analyzed by [20] in the context of linear elasticity. These authors obtained microstructures known as *coated spheres assemblages* or *Hashin-Shtrikman micro-structures* that provide lower and upper bounds for the elastic properties of bi-material composites. In the present context of heat conducting materials, the upper bound corresponds to a microstructure consisting of disks of the lower conductivity phase coated by a layer (ring) of the higher conductivity material. For the lower bound, the disks and rings are made respectively of the higher and lower conductivity materials. In the present example, the upper bound is retrieved.

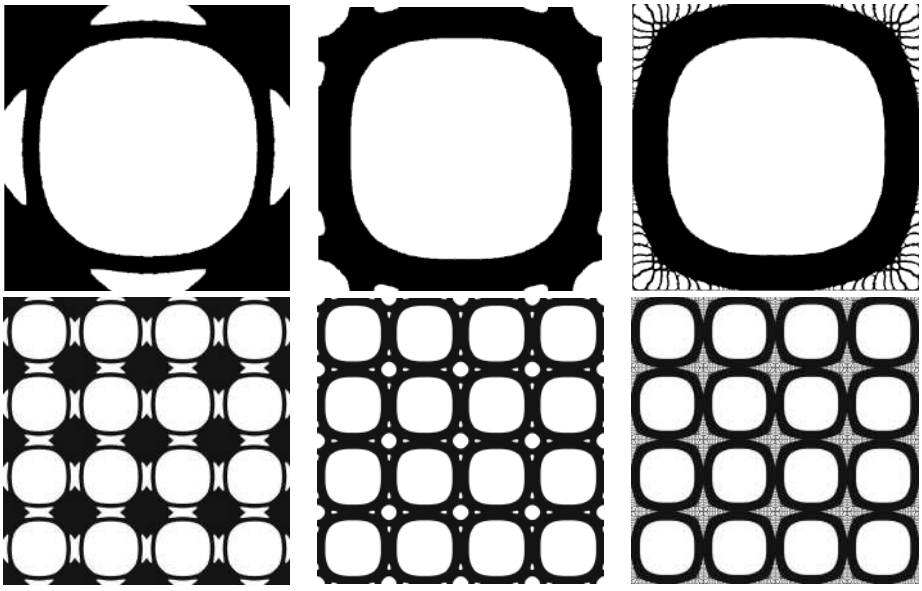

(a) linear model (b) periodic model (c) uniform model

FIGURE 7. Orthotroic heat conductivity maximization.

topology	homogenization model for computation of h		
generated with	linear	periodic	uniform
linear	3.24	4.54	7.03
periodic	3.54	3.61	6.11
uniform	3.63	3.64	3.66

TABLE 1. Orthotropic heat conduction maximization. Value of function h using different homogenization models for the obtained optimized topologies.

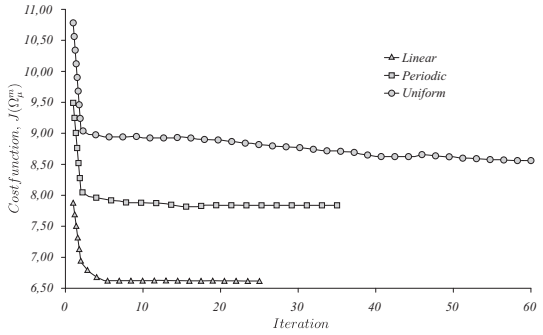

FIGURE 8. Orthotropic heat conductivity maximization.

A further insight into the influence of the choice of homogenization model on the properties of the obtained optimized topologies can be gained from Table 1. For each of the three optimized topologies obtained (corresponding to the rows of the table), the value of the function h (that measures the property to be minimized) are computed according to the linear, periodic and uniform flux boundary conditions. The columns shows that the minimum value of h computed according to a particular model corresponds to the topology optimized having the same model as the estimator of the macroscopic properties. That is, as one should expect, the algorithm synthesizes topologies that are closer to the optimum in the particular metric defined by the chosen homogenization model. Another interesting fact is that very little difference among the values of h computed according to the three models is observed for the more complex topology generated using the uniform boundary flux model (the last row of the table). As the homogenization process using the linear (uniform) model provides an upper (lower) bound for the conductivity tensor components (upon which h depends), this tight variation in the bounds of h suggests a higher degree of reliability of the predicted optimized property obtained by the algorithm with the uniform model in this case (note that large variations in the predicted h occur for the other topologies).

5.3. **Horizontal rigidity maximization.** In this first numerical example of elastic microstructure optimization, we consider the function $h(\mathbb{C})$ given by

$$h(\mathbb{C}) := (\mathbb{C}^{-1})_{1111}. \tag{5.3}$$

Its minimization corresponds to the maximization of the longitudinal elastic modulus. The Lagrange multiplier is chosen as $\lambda = 30$. The optimized topologies for each multi-scale model considered are shown in fig. 9 and the convergence history of the cost function can be seen in fig. 10.

(a) linear model (b) periodic model (c) uniform model

FIGURE 9. Horizontal rigidity maximization.

The topologies presented in figs. 9(a) and 9(b) coincide with the classical topology proposed by [44] and [36] as an upper bound for the overall elastic modulus, where the stiffer material is aligned with the direction along which the maximization of the elastic modulus is sought (refer to comments made in example 5.1). Again, it should be noted that the topology obtained under the uniform boundary traction assumption (minimal kinematical constraint) is far more complex than the ones generated under the more kinematically constrained assumptions.

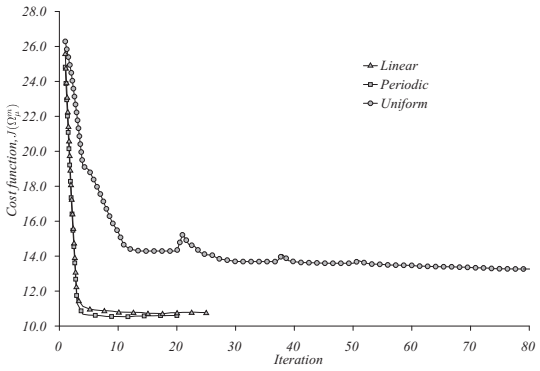

FIGURE 10. Horizontal rigidity maximization. Convergence history.

5.4. **Bulk modulus maximization.** To maximize the bulk modulus, we define

$$h(\mathbb{C}) := (\mathbb{C}^{-1})_{1111} + 2(\mathbb{C}^{-1})_{1122} + (\mathbb{C}^{-1})_{2222}. \tag{5.4}$$

The volume fraction of inclusion material is fixed as 0.32 and the parameter λ determined accordingly. The corresponding optimized topologies are shown in fig. 11 and the convergence history of the cost function is depicted in fig. 12.

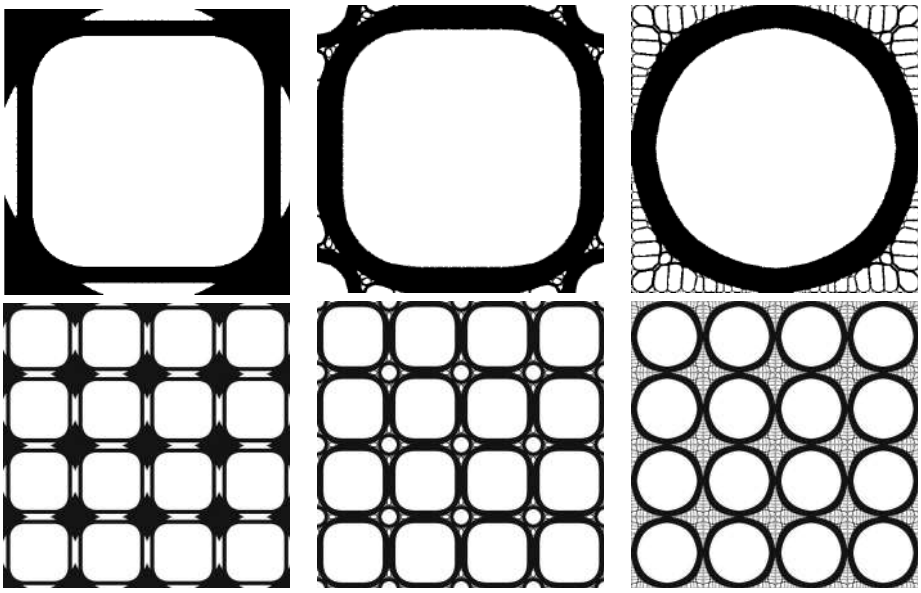

(a) linear model (b) periodic model (c) uniform model

FIGURE 11. Bulk modulus maximization.

The topologies obtained for the linear and periodic models are very similar to the one analyzed by [20].

FIGURE 12. Bulk modulus maximization. Convergence history.

The upper bound topologies synthesized is these cases are of the *coated spheres assemblage* type or *Hashin-Shtrikman micro-structure* ([5, 30]). They consist of disks of the most compliant material coated with rings of stiffer material. The optimized RVE obtained under the uniform boundary traction assumption is of particular resemblance to the *coated spheres assemblage* of [20]. The result suggests a fractal nature of the optimum microstructure whose details are captured with higher resolution in the optimization process as the mesh is refined. Similarly to the analysis conducted in the orthotropic heat conductivity example (refer to Table 1), we plot in Table 2 the values of the function h using the three homogenization models for each of the optimized microstructures obtained. The conclusions here are analogous to those of the heat conduction counterpart example. In particular, here we also find that the the use of the uniform boundary traction model in the optimization algorithm yields a microstructural topology whose lower and upper bounds (related to the last row of Table 2) for the predicted optimized property (the bulk modulus in the present case) are very close and, hence, appears to provide a more reliable indication of the actual optimal topology.

topology	homogenization model for computation of h		
generated with	linear	periodic	uniform
linear	8.01	10.58	26.70
periodic	9.16	9.30	18.27
uniform	9.32	9.34	9.46

TABLE 2. Bulk modulus maximization. Value of function h using different homogenization models for the obtained optimized topologies.

5.5. **Shear modulus maximization.** For the maximization of the shear modulus, we define simply

$$h(\mathbb{C}) := 4(\mathbb{C}^{-1})_{1212}. \tag{5.5}$$

The volume fraction of inclusion is fixed as 0.70. The optimized topologies obtained for each multi-scale model are shown in fig. 13 and the convergence history of the correponding cost function is plotted in fig. 14.

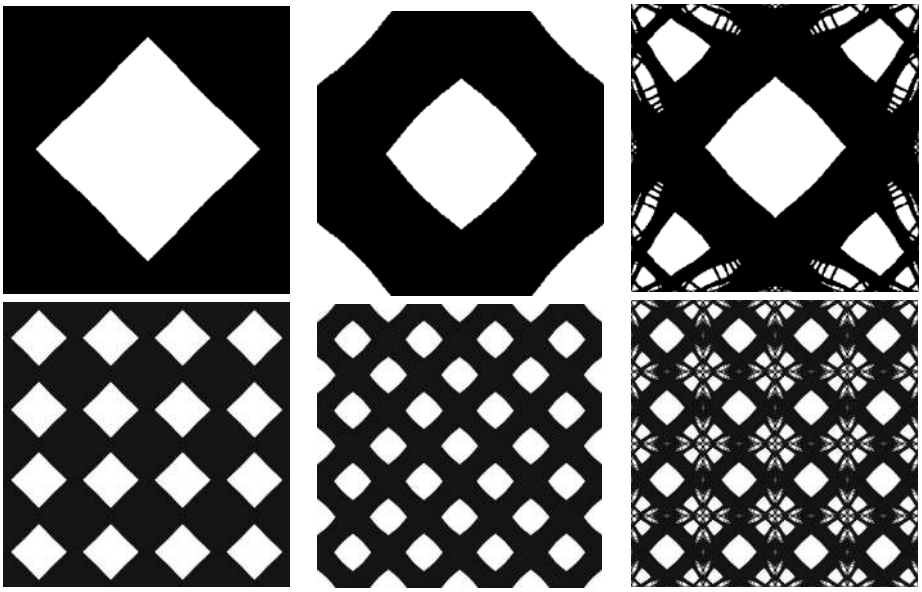

(a) linear model (b) periodic model (c) uniform model

FIGURE 13. Shear modulus maximization.

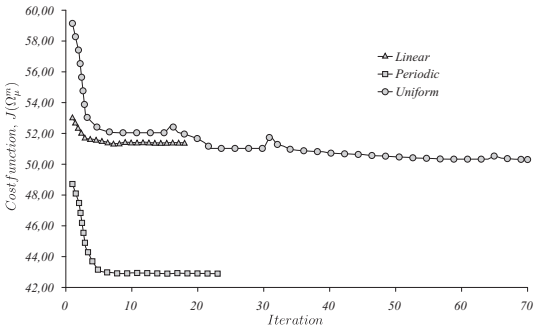

FIGURE 14. Shear modulus maximization. Convergence history.

Again, the topology obtained for the minimally constrained model are of a far greater complexity than the ones obtained with the less kinematically constrained models. It is worth mentioning that here we also observed that, similarly to the results reported in Tables 1 and 2, the smallest difference between the upper and lower bounds for the shear modulus (a difference of 6%) occurs for the optimized topology obtained under the minimally constrained (uniform boundary traction) assumption.

5.6. **Poisson's ratio minimization.** Here we consider the definition

$$h(\mathbb{C}) := -(\mathbb{C}^{-1})_{1122}, \tag{5.6}$$

and take $\lambda = 0.5$. The optimized topologies are shown in fig. 15 and the convergence behaviour of the cost function can be seen in fig. 16.

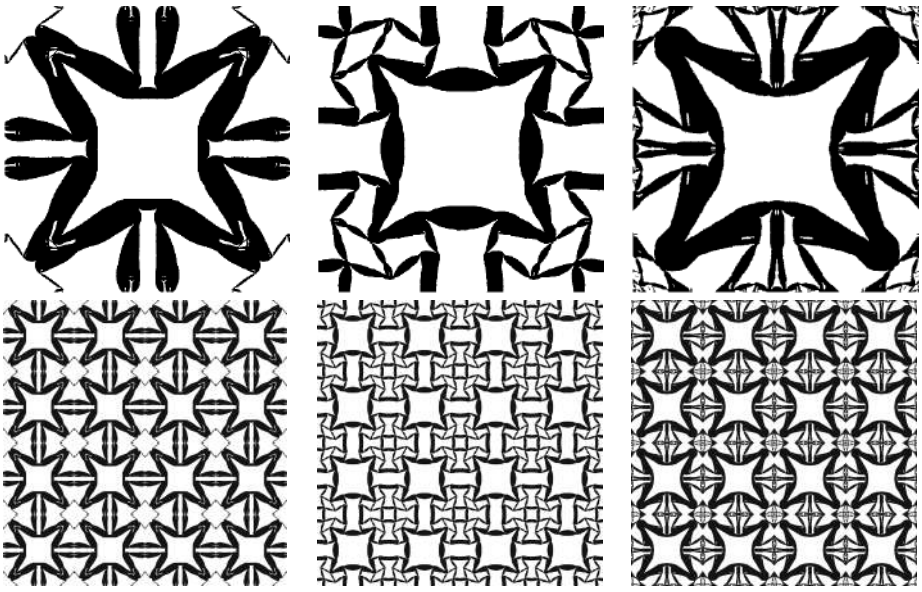

(a) linear model (b) periodic model (c) uniform model

FIGURE 15. Poisson's ratio minimization.

The corresponding homogenized elasticity tensors in matrix representation are

$$\begin{aligned} C^{\mathcal{L}} &= \begin{pmatrix} 0.0663 & -0.0243 & 0 \\ -0.0243 & 0.0663 & 0 \\ 0 & 0 & 0.0127 \end{pmatrix}, \\ C^{\mathcal{P}} &= \begin{pmatrix} 0.0718 & -0.0302 & 0 \\ -0.0302 & 0.07018 & 0 \\ 0 & 0 & 0.0084 \end{pmatrix}, \\ C^{\mathcal{U}} &= \begin{pmatrix} 0.0698 & -0.0250 & 0 \\ -0.0250 & 0.0698 & 0 \\ 0 & 0 & 0.0123 \end{pmatrix}, \end{aligned} \tag{5.7}$$

respectively, for the linear, periodic and minimally constrained models. The associated Poisson's ratios are negative in al cases:

$$\nu^{\mathcal{L}} = -0.366, \quad \nu^{\mathcal{P}} = -0.421 \quad \text{and} \quad \nu^{\mathcal{U}} = -0.359. \tag{5.8}$$

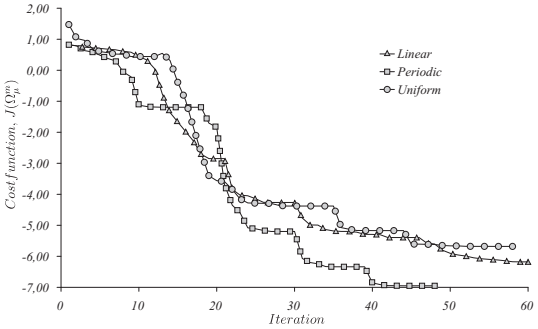

FIGURE 16. Poisson's ratio minimization. Convergence history.

The results show that, regardless of the particular class of multi-scale model used to predict the macroscopic response, the optimized microstrucre features the auxetic behavior of the star-shaped encapsulated inclusions, analyzed by, among others, by [2, 26, 42, 41]. This type of micro-cell is known as *nonconvex-shaped* or *re-entrant corner* microstructures.

5.7. **Poisson's ratio maximization.** The target in this last example is the maximization of the Poisson'r ratio. In the corresponding cost function we define

$$h(\mathbb{C}) := \frac{(\mathbb{C}^{-1})_{1122}}{(\mathbb{C}^{-1})_{1111}} + \frac{(\mathbb{C}^{-1})_{1122}}{(\mathbb{C}^{-1})_{2222}}\,. \tag{5.9}$$

Again, we choose $\lambda = 0.5$. The results for all multi-scale models adopted are shown in fig. 17. The history of the cost function throughout the optimization iterations is plotted in the graph of fig. 18. The matrix representation of the corresponding homogenized elasticity tensor at the end of the optimization process is given by

$$\begin{aligned} C^{\mathcal{L}} &= \begin{pmatrix} 0.0734 & 0.0599 & 0 \\ 0.0599 & 0.0734 & 0 \\ 0 & 0 & 0.0364 \end{pmatrix}, \\ C^{\mathcal{P}} &= \begin{pmatrix} 0.0849 & 0.0714 & 0 \\ 0.0714 & 0.0849 & 0 \\ 0 & 0 & 0.0265 \end{pmatrix}, \\ C^{\mathcal{U}} &= \begin{pmatrix} 0.1233 & 0.1072 & 0 \\ 0.1072 & 0.1233 & 0 \\ 0 & 0 & 0.0453 \end{pmatrix}. \end{aligned} \tag{5.10}$$

which results in the Poisson's ratios:

$$\nu^{\mathcal{L}} = 0.816, \quad \nu^{\mathcal{P}} = 0.841 \quad \text{and} \quad \nu^{\mathcal{U}} = 0.870. \tag{5.11}$$

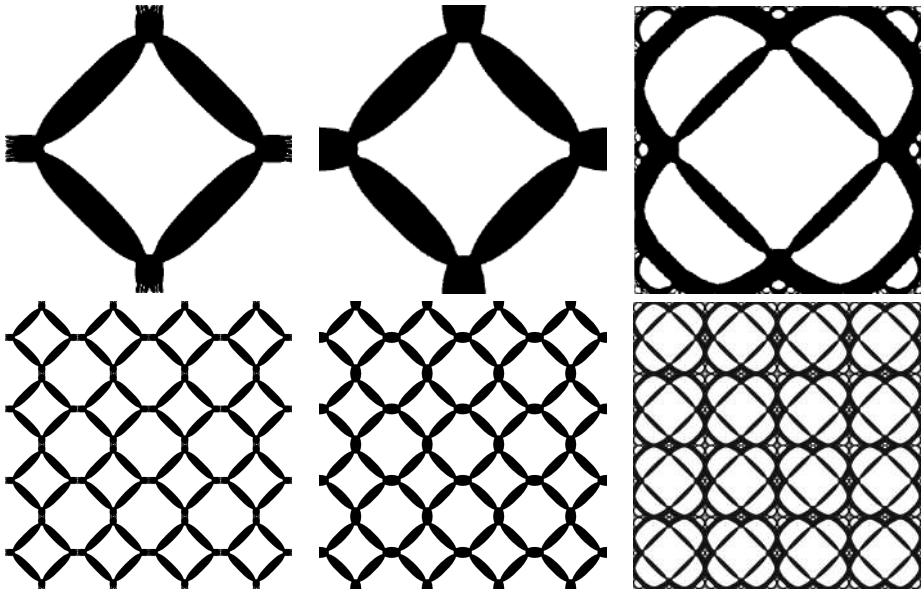

(a) linear model (b) periodic model (c) uniform model

FIGURE 17. Poisson's ratio maximization.

FIGURE 18. Poisson's ratio maximization. Convergence history.

We observe here that for the three multi-scale models considered exhibit, the synthesized microstructure at the end of the optimization procedure has a *pantograph-like* topology. This type of microstructure allows a maximum transfer of strain energy from one direction to the direction orthogonal to it.

6. Conclusions

A microstructural optimization algorithm based on the concept of topological derivative and a level-set domain representation has been applied to the synthesis of elastic and heat conducting bi-material microstructures. For comparison, different multi-scale constitutive models have been used in the estimation of the macroscopic material properties of interest to the optimization process: (a) the classical periodic boundary constraint model, typical of the description of periodic media; (b) the linear boundary constraint model which provides an upper bound for the macroscopic heat conductivity and elasticity tensors; and (c) the minimum constraint model which, in turn, provides a lower bound for these tensors. The study has shown that the final optimized topology synthesized by the algorithm depends (sometimes strongly) on the particular model adopted. In particular, the use of the minimally constrained model generally leads to more complex optimized topologies. Interestingly, the results also appear to suggest that the optimized macroscopic properties for such more complex topologies lie within tighter bounds

than those obtained with the the linear and periodic boundary constraint models. Further investigation is currently under way to establish the extent of such a tendency.

Acknowledgements

This research was partly supported by the Royal Society International Joint Project JP080066. S.M. Giusti was supported by CNPq (Brazilian Research Council) under the Grant 382485/2009-2. This support is gratefully acknowledged.

References

[1] G. Allaire, F. Jouve, and A.M. Toader. Structural optimization using sensitivity analysis and a level-set method. *Journal of Computational Physics*, 194(1):363–393, 2004.

[2] R.F. Almgreen. An isotropic three-dimensional structure with Poisson's ratio -1. *Journal of Elasticity*, 15(4):427–430, 1985.

[3] S. Amstutz and H. Andrä. A new algorithm for topology optimization using a level-set method. *Journal of Computational Physics*, 216(2):573–588, 2006.

[4] S. Amstutz, I. Horchani, and M. Masmoudi. Crack detection by the topological gradient method. *Control and Cybernetics*, 34(1):81–101, 2005.

[5] P. Avserth, T. Mukerji, and G. Mavko. *Quantitative seismic interpretation: applying rock physics tools to reduce interpretation risk*. Cambridge University Press, Cambridge, 2005.

[6] T. Belytschko, S. Xiao, and C. Parimi. Topology optimization with implicit functions and regularization. *International Journal for Numerical Methods in Engineering*, 57:1177–1196, 2003.

[7] M. P. Bendsøe and O. Sigmund. *Topology optimization. Theory, methods and applications*. Springer-Verlag, Berlin, 2003.

[8] A. Bensoussan, J.L. Lions, and G. Papanicolau. *Asymptotic analysis for periodic microstructures*. North Holland, Amsterdam, 1978.

[9] J. Céa, S. Garreau, Ph. Guillaume, and M. Masmoudi. The shape and topological optimizations connection. *Computer Methods in Applied Mechanics and Engineering*, 188(4):713–726, 2000.

[10] E.A. de Souza Neto and R.A. Feijóo. Variational foundations of multi-scale constitutive models of solid: small and large strain kinematical formulation. Technical Report No 16/2006, Laboratório Nacional de Computação Científica LNCC/MCT, Petrópolis, Brasil, 2006.

[11] J.D. Eshelby. The determination of the elastic field of an ellipsoidal inclusion, and related problems. *Proceedings of the Royal Society: Section A*, 241(1226):376–396, 1957.

[12] S. Garreau, Ph. Guillaume, and M. Masmoudi. The topological asymptotic for pde systems: the elasticity case. *SIAM Journal on Control and Optimization*, 39(6):1756–1778, 2001.

[13] P. Germain, Q.S. Nguyen, and P. Suquet. Continuum thermodynamics. *Journal of Applied Mechanics, Transactions of the ASME*, 50(4):1010–1020, 1983.

[14] S.M. Giusti, P.J. Blanco, E.A. de Souza Neto, and R.A. Feijóo. An assessment of the Gurson yield criterion by a computational multi-scale approach. *Engineering Computations*, 26(3):281–301, 2009.

[15] S.M. Giusti, A.A. Novotny, and E.A. de Souza Neto. Sensitivity of the macroscopic response of elastic microstructures to the insertion of inclusions. *Proceeding of the Royal Society: Section A*, doi:10.1098/rspa.2009.0499, 2010.

[16] S.M. Giusti, A.A. Novotny, E.A. de Souza Neto, and R.A. Feijóo. Topological derivative in multi-scale linear elasticity models. In 8^{th} *World Congress on Computational Mechanics and* 5^{th} *European Congress on Computational Methods in Applied Sciences and Engineeering, WCCM-ECCOMAS Proceedings*, Venice, Italy, 2008.

[17] S.M. Giusti, A.A. Novotny, E.A. de Souza Neto, and R.A. Feijóo. Sensitivity of the macroscopic elasticity tensor to topological microstructural changes. *Journal of the Mechanics and Physics of Solids*, 57(3):555–570, 2009.

[18] S.M. Giusti, A.A. Novotny, E.A. de Souza Neto, and R.A. Feijóo. Sensitivity of the macroscopic thermal conductivity tensor to topological microstructural changes. *Computer Methods in Applied Mechanics and Engineering*, 198(5-8):727–739, 2009.

[19] A.L. Gurson. Continuum theory of ductile rupture by void nucleation and growth: Part i – yield criteria and flow rule for porous ductile media. *Journal Engineering Materials and Technology – Transactions of the ASME*, 99(1):2–15, 1977.

[20] Z. Hashin and S. Shtrikman. A variational approach to the theory of the elastic behaviour of multiphase materials. *Jounal of the Mechanics and Physics of Solids*, 11(2):127–140, 1963.

[21] R. Hill. A self-consistent mechanics of composite materials. *Journal of the Mechanics and Physics of Solids*, 13(4):213–222, 1965.

[22] M. Hintermüller and A. Laurain. Electrical impedance tomography: from topology to shape. *Control and Cybernetics*, 37(4):913–933, 2008.

[23] M. Hintermüller and A. Laurain. Multiphase image segmentation and modulation recovery based on shape and topological sensitivity. *Journal on Mathematical Imaging and Vision*, 35:1–22, 2009.

[24] S. Hyun and S. Torquato. Designing composite microstructures with targeted properties. *Journal of Materials Research*, 16(1):280–285, 2001.

[25] N. Kikuchi, S. Nishiwaki, J.S.O. Fonseca, and E.C.N. Silva. Design optimization method for compliant mechanisms and material microstructure. *Computer Methods in Applied Mechanics and Engineering*, 151(3-4):401–417, 1998.

[26] R. Lakes. Foam structures with negative Poisson's ratio. *Science, AAAS*, 235(4792):1038–1040, 1987.
[27] J. Mandel. *Plasticité classique et viscoplasticité*. CISM Lecture Notes. Springer-Verlag, Udine, 1971.
[28] J.C. Michel, H. Moulinec, and P. Suquet. Effective properties of composite materials with periodic microstructure: a computational approach. *Computer Methods in Applied Mechanics and Engineering*, 172(1-4):109–143, 1999.
[29] C. Miehe, J. Schotte, and J. Schröder. Computational micro-macro transitions and overall moduli in the analysis of polycrystals at large strains. *Computational Materials Science*, 16(1-4):372–382, 1999.
[30] G.W. Milton. *The Theory of Composites*. Number 6 in Cambridge Monographs on Applied and Computational Mathematics. Cambridge University Press, Cambridge, UK, 2002.
[31] S.A. Nazarov and J. Sokołowski. Asymptotic analysis of shape functionals. *Journal de Mathématiques Pures et Appliquées*, 82(2):125–196, 2003.
[32] A.A. Novotny, R.A. Feijóo, E. Taroco, and C. Padra. Topological sensitivity analysis for three-dimensional linear elasticity problem. *Computer Methods in Applied Mechanics and Engineering*, 196(41-44):4354–4364, 2007.
[33] M. Ostoja-Starzewski and J. Schulte. Bounding of effective thermal conductivities of multiscale materials by essential and natural boundary conditions. *Physical Review B*, 54(1):278–285, 1996.
[34] I. Özdemir, W. Brekelmans, and M. Geers. Computational homogenization for heat conduction in heterogeneous solids. *International Journal for Numerical Methods in Engineering*, 73(2):185–204, 2008.
[35] G. Pólya and G. Szegö. *Izoperimetric inequalities in mathematical physics*. Princeton University Press, Princeton, 1951.
[36] A. Reuss. Berechnung der fliessgrenze von mischkristallen auf grund der plastizitätsbedingung für einkristalle. *Zeitschrift für Angewandte Mathematik und Mechanik*, 9:49–58, 1929.
[37] E. Sanchez-Palencia. *Non-homogeneous media and vibration theory*, volume 127 of *Lecture Notes in Physics 127*. Springer-Verlag, Berlin, 1980.
[38] O. Sigmund. Materials with prescribed constitutive parameters: an inverse homogenization problem. *International Journal Solids and Structures*, 31(17):2313–2329, 1994.
[39] E.C.N. Silva, J.S.O. Fonseca, and N. Kikuchi. Optimal design of periodic microstructures. *Computational Mechanics*, 19(5):397–410, 1997.
[40] J. Sokołowski and A. Żochowski. On the topological derivative in shape optimization. *SIAM Journal on Control and Optimization*, 37(4):1251–1272, 1999.
[41] G.E. Stavroulakis. Auxetic behaviour: appearance and engineering applications. *Physica Status Solidi b*, 242(3):710–720, 2005.
[42] P.S. Theocaris, G.E. Stavroulakis, and P.D. Panagiotopoulos. Negative Poisson's ratios in composites with star-shaped inclusions: a numerical homogenization approach. *Archive of Applied Mechanics*, 67(4):274–286, 1997.
[43] I. Turevsky, S.H. Gopalakrishnan, and K. Suresh. An efficient numerical method for computing the topological sensitivity of arbitrary-shaped features in plate bending. *International Journal for Numerical Methods in Engineering*, 79(13):1683–1702, 2009.
[44] W. Voigt. Über die beziehung zwischen den beiden elastizitätskonstanten isotroper körper. *Wiedemann Annalen*, 38:573–587, 1889.
[45] J.R. Willis. Variational and related methods for the overall properties of composites. *Advances in Applied Mechanics*, 21:1–78, 1981.

(E.A. de Souza Neto) Civil and Computational Engineering Centre, School of Engineering, Swansea University, SingletonPark, Swansea SA28PP, UK
E-mail address: E.deSouzaNeto@swansea.ac.uk

(S. Amstutz) Laboratoire d'analyse non linéaire et géométrie, Faculté des Sciences, 33 rue Louis Pasteur, 84000 Avignon, France.
E-mail address: samuel.amstutz@univ-avignon.fr

(S.M. Giusti) Laboratório Nacional de Computação Científica LNCC/MCT, Coordenação de Matemática Aplicada e Computacional, Av. Getúlio Vargas 333, 25651-075, Petrópolis - RJ, Brasil
E-mail address: giusti@lncc.br

(A.A. Novotny) Laboratório Nacional de Computação Científica LNCC/MCT, Coordenação de Matemática Aplicada e Computacional, Av. Getúlio Vargas 333, 25651-075 Petrópolis - RJ, Brasil.
E-mail address: novotny@lncc.br